*energies*

MDPI

*Article*

# Kinetic and Thermodynamic Study of the Wet Desulfurization Reaction of ZnO Sorbents at High Temperatures

**Erwin Ciro [1], Alessandro Dell'Era [2,*], Arda Hatunoglu [1,3], Enrico Bocci [1] and Luca Del Zotto [4,*]**

[1] Department of Engineering Sciences, Università degli Studi Guglielmo Marconi, 00193 Rome, Italy
[2] Department of Basic and Applied Science for Engineering, Sapienza University of Rome, 00161 Rome, Italy
[3] Department of Astronautics, Electrical and Energy Engineering, Sapienza Università di Roma, Via Eudossiana 18, 00184 Rome, Italy
[4] Centro di Ricerca su Energia, Ambiente e Territorio, Università Telematica eCampus, 22060 Novedrate, Italy
* Correspondence: alessandro.dellera@uniroma1.it (A.D.); luca.delzotto@uniecampus.it (L.D.Z.)

**Abstract:** Hot gas conditioning is a remarkable stage for decreasing typical and harsh contaminants of syngas produced in the biomass gasification process. Downstream contaminants containing hydrogen sulphide ($H_2S$) can significantly deteriorate fuel stream conversion reactors and fuel cell systems. Thus, an effective gas cleaning stage is required to remove critical streams that endanger the whole pathway toward the biomass conversion process. In this work, we studied $H_2S$ capture from biofuel syngas by using a kinetic deactivation model to analyze the effect of the operating conditions on the adsorption performance. Furthermore, the particle sorbent influence on other reactions, such as methane reforming and water gas shift (WGS), were also evaluated. Breakthrough curves were plotted and fitted following a first-order linearized deactivation model to perform both the $H_2S$ adsorption capacity and thermodynamic analysis. Moreover, the influence of the operating conditions was studied through a breakthrough curve simulation. By using the Arrhenius and Eyring–Polanyi expressions, it was possible to calculate the activation energy and some thermodynamic parameters from the transition state theory. Finally, a mathematical analysis was performed to obtain the diffusion coefficient ($D$) and the kinetic reaction constant ($\bar{k}_0$) of $H_2S$ gas within ZnO particles, considering a spherical geometry.

**Keywords:** desulfurization; deactivation model; ZnO sorbent; thermodynamic analysis; hot gas conditioning; breakthrough curves



**Citation:** Ciro, E.; Dell'Era, A.; Hatunoglu, A.; Bocci, E.; Del Zotto, L. Kinetic and Thermodynamic Study of the Wet Desulfurization Reaction of ZnO Sorbents at High Temperatures. *Energies* **2023**, *16*, 792. https://doi.org/10.3390/en16020792

Academic Editor: Eliseu Monteiro

Received: 2 December 2022
Revised: 27 December 2022
Accepted: 30 December 2022
Published: 10 January 2023



## 1. Introduction

Hot gas conditioning (HGC) is an intermediate stage to capture critical contaminants in fuel gas conversion to useful electricity. Such pollutants can endanger efficient downstream production of liquid biofuels, electricity, and heat within integrated membrane reactors and cell systems, putting at risk the environment and the occupational safety of workers [1,2]. The synthesis gas from biomass gasification, also known as syngas, is a mixture of $H_2$, CO, $CO_2$, and $CH_4$, and it is recognized to be a potential energetic source to supply the current power demand. Initially, raw syngas usually contains contaminant concentrations of tars, organic compounds ($C_6H_6$, $C_{10}H_8$, and $C_{14}H_{10}$), sulphur ($H_2S$, COS, $CS_2$, and $C_4H_4S$), halogens (HCl, HF, HBr, and $SnCl_2$), nitrides ($NH_3$, HCN, and $N_2$), and alkali metals [1,3]. In particular, one of the most critical contaminants is hydrogen sulphide ($H_2S$), which can reach a broad concentration (up to 0.5 g $kg^{-1}$) within biomass feedstocks [4]. This concentration, which is even lower than that observed from coal (50 g $kg^{-1}$), can compromise the whole performance and lifetime process due to the high corrosion and poisoning of reformers, burners, tanks, pipelines and the structural elements in a solid oxide fuel cell (SOFC) [4,5]. Thus, $H_2S$ abatement downstream of the gasification process is gaining attention for developing reliable and effective treatments to achieve clean fuel gas.

Mature technologies for pollutant removal have been associated with catalytic combustion [6,7], oxidation [8], acid gas treatment, and adsorption, of which their actual effectiveness at high temperatures (above 500 °C) is highlighted in $H_2S$ removal. In contrast, other techniques at lower temperatures, such as condensation [9] and carbon-activated adsorption [10], are less attractive due to the subsequent cooling/heating stages, turning into inefficient energetic strategies if the goal is sustainable fuel gas production. In this context, exothermic features and $H_2S$ adsorption capacity to form metal sulphides at high temperatures make thermochemical adsorption one of the most utilized methodologies to desulfurize syngas [4].

From the literature, thermochemical adsorption occurs when metal oxide sorbents are in contact with $H_2S$ contaminated streams. In this context, sorbents should respect some requirements to achieve the complete $H_2S$ capture, which include: (i) large specific area, (ii) efficient sulfidation reaction (high equilibrium constant) and fast kinetics, (iii) resistance to the reductive atmosphere, (iv) low cost, and (v) low losses by attrition [11,12]. Then, different oxides have been classified due to their $H_2S$ capture ability in a wide range of temperatures (77 to 650 °C), as follows: Sn < Ni < Fe < Mn < Mo < Co < Zn < Cu and Ce [13]. CeO and CuO exhibit notable desulfurization capacity (g sulphur/g sorbent). On the one hand, for instance, reduced non-stoichiometric CeO at 800 °C is broadly considered to be a superior sorbent to $CeO_2$, having shown the ability to decrease $H_2S$ concentration in less than 20 ppmv and a lifetime of twenty-five desulfurization cycles. However, an imbalance between additional reductive thermal treatments and high prices is a common challenge that must be tackled [1,3]. Likewise, copper oxide can be used to perform $H_2S$ removal under reducing and oxidizing conditions. The reducing atmosphere is much more catastrophic since a rapid conversion from oxide to metallic copper is achieved. In addition, once the metallic copper is formed, it cannot thermodynamically react with sulphur at high temperatures. Thereby, copper-based sorbents such as Cu-V and Cu-Mo in a fixed-bed column have shown a slower reduction reaction (from CuO to Cu) [14].

On the other hand, zinc oxide (ZnO) has been assessed by maintaining a suitable compromise between operative conditions and the above-mentioned features for the desulfurization reaction [2]. In the literature, by varying operative parameters (temperature, bed length, flow rate, compositions of both sorbent and syngas), the $H_2S$ adsorption by ZnO-based sorbents has been affected. Hence, low-temperature ranges (300–400 °C) have captured $H_2S$ suitably (less than 20 ppbv at the bed-reactor outlet) without altering the sorbent integrity [15]. Although some studies have reported proper functionality even at 550 °C, temperatures beyond 700 °C could cause an undesirable effect, i.e., Zn vaporization. Moreover, the composition of syngas can compromise $H_2S$ capture, that is, excess steam can cause an evident left shift of the equilibrium reaction favoring ZnO and $H_2S$ formation, while additional $CO_2$ presence can cause an inhibiting effect that can be attributed to competitive adsorption phenomena between $CO_2$ and $H_2S$ [16].

The composition of the sorbent can also cause significant variations in the capture effectiveness. ZnO sorbents containing dolomite/Zn-Ni and Cu-Zn/$SiO_2$ have been used at temperatures between 300 and 400 °C, while using Fe and Ti metal oxide additions can achieve plausible outcomes above 600 °C [12,17]. Other metal oxide types ($SiO_2$, $ZrO_2$, and $Al_2O_3$) containing 5–15 wt.% $ZnMn_2O_4$ additions have been assessed between 500 and 700 °C with gas hourly space velocity (GHSV) and inlet concentration at 2000 $h^{-1}$ and 10% of $H_2S$, respectively. Complete saturation has been reached after 15 min at 600 °C with the formation of ZnS, MnS, and $Mn_{0.6}Zn_{0.4}S$ at the end of the process. In this case, the calculated activation energy ($E_a$) for the $H_2S$ capture was 98.8 kJ $mol^{-1}$ [18]. Likewise, novel sorbent materials have been introduced, sometimes incorporating a catalytic effect during $H_2S$ capture. Others seek higher stabilization at higher temperatures to hinder metal evaporation [15,19]. In such cases, the former has adopted internal porosity with different 3D structure mesoporous molecular and ZnO loadings to increase active sites and to enhance the diffusion of the gas–solid reaction [15,19]. The latter has proposed mixtures of ZnO sorbents doped with refractory oxides to form spinel, perovskite-like materials

that have much more resistance against the reduction reaction and high adsorption and regeneration responses [20]. Different scopes and operative conditions have been generally considered to study sulphur removal using ZnO sorbent in hot gas conditioning during biomass gasification. A summary of the most recent and related works is listed in Table 1.

**Table 1.** Summary of the main contribution of the latest works on sulphur removal using ZnO-based sorbents.

| Sorbent | Year | Highlights | Ref. |
|---|---|---|---|
| ZnO | 2022 | - Syngas + 260 ppmv $H_2S$ + 20% $H_2O$ at different GHVS (25,000–50,000 $h^{-1}$) and temperatures (450–600 °C);<br>- Thermodynamic and kinetic analysis;<br>- Simulation of operating conditions and bed sizing;<br>- Kinetic analysis using spherical coordinates. | This work |
| | 2021 | - $N_2$ + 410 ppmv $H_2S$ + 18% $H_2O$ at different GHVS (25,000–50,000 $h^{-1}$), and temperatures (400–600 °C);<br>- Thermodynamic and kinetic analysis;<br>- Sorbent characterization (SEM, EDS, BET, and XRD). | [21] |
| | 2020 | - Two types of syngas + (100 to 120 ppmv) $H_2S$ + ~30% $H_2O$ at different GHVS (17,000–26,000 $h^{-1}$), temperatures (300–400 °C), particle size (1.0−1.25 and 2.0−2.38 mm);<br>- Kinetic analysis;<br>- Sorbent characterization (SEM, Optical analysis). | [22] |
| | 2015 | - Fluidized bed gasification above 800 °C;<br>- Filtration 300 °C;<br>- Removal of $H_2S$ at 300 °C/regeneration around 700 °C;<br>- Steam reforming of tar. | [23] |
| | 2010 | - He + 1% $H_2S$ and dry conditions at GHVS of 47,750 $h^{-1}$ and different temperatures (60–400 °C);<br>- Regeneration reaction above 700 °C;<br>- Sorbent characterization (XRD, BET specific surface area, pore volume, SEM/EDX, TGA/DSC, and in situ XRD). | [15] |
| | 2007 | - Biogas + (100–800 ppmv) $H_2S$ + 45% $H_2O$ at different GHVS (8000–240,000 $h^{-1}$), temperatures (250–365 °C), and particle size (0.15−0.250 to 0.425−1 mm);<br>- Study of the effect of operative conditions. | [24] |
| Zeolite with 10%, 20%, 30% and 100% ZnO | 2018 | - $N_2$ + 200 ppmv $H_2S$ at room temperature;<br>- Physicochemical performance of different prepared sorbent mixtures;<br>- Regeneration tests - sorbent characterization (SEM, EDAX, XRD, FTIR, Nitrogen adsorption/desorption isotherms). | [25] |
| Zn-Co-Ti-O based sorbent | 2016 | - Sorbent synthesis and characterization (XRD, SEM–EDX, XPS, mercury porosimetry, and TPRH2). | [20] |
| Zn–Mn sorbent | 2007 | - Syngas + 10% $H_2S$ + 20% $H_2O$ at GHVS of 6000 mL $h^{-1}$ $g^{-1}$, and different temperatures (300–700 °C);<br>- Synthesis and characterization of sorbents (XRD and BET);<br>- Thermodynamic and kinetic analysis. | [18] |

In our previous work, ZnO-based sorbents were used to evaluate wet desulfurization using hydrogen and steam in a wide range of temperatures between 400 and 600 °C with GHSV between 25,000 and 50,000 $h^{-1}$. The best result indicated that ZnO sorbents could adsorb around 5.4 g per 100 g of the sorbent at 550 °C [21]. The linearized deactivation model calculated the initial adsorption rate constant ($k_s$*) and the deactivation rate constant

($k_d$) for each thermal condition. At the same time, the $E_a$ for this experimental system was about 10 kJ mol$^{-1}$. From this work, it was also possible to indicate that intraparticle diffusional resistances and intraparticle mass transfer limitations were not negligible [21]. Since flow gas was fixed with $N_2$-diluted hydrogen and $H_2S$ mixtures, the analysis of breakthrough curves using quite similar conditions to those found inside an HGC reactor would be relevant to understanding thermodynamic and kinetic responses in a more realistic environment.

Based on previous results and methodology, in this work, we attempt to understand the effect of the desulfurization reaction using ZnO sorbents in terms of the thermodynamic constants and to analysis a kinetic deactivation model for the wet desulfurization reaction via ZnO at different temperatures in the presence of syngas in a temperature range between 450 and 600 °C. Therefore, the novelty of this work is focused on studying ZnO sorbent performance using syngas, in different operating conditions, to determine thermodynamic and kinetic parameters, which contribute to estimate the sizing of a bed length and to analyze some critical aspects. Further, a modeling of the breakthrough curve considering the operating parameters together with a spherical model of adsorption inside the particles allow us to determine the gas intraparticle diffusion coefficient and kinetic reaction $k_0$, increasing the data available in the literature.

## 2. Materials and Methods

The experimental campaign was conducted using a custom-made U-shaped quartz reactor at atmospheric pressure with inner and outer diameters of 8.0 and 12.3 mm, respectively. ZnO particle sorbent, showing a distribution size between 1.5 and 3.0 mm and 0.714 g cm$^{-3}$ density, was put within the U-shaped quartz reactor with a length of bed (LB) defined as 0.8 and 1.5 cm. The physical features of ZnO particles are presented in Table 2.

**Table 2.** Properties of ZnO sorbents.

| Features | Outputs |
|---|---|
| Type | Spherical |
| Activation | High temperatures in the presence of steam |
| Particle size (mm) | 1.5–3.0 |
| BET surface (m$^2$ g$^{-1}$) | 43 [21] |
| Density (g cm$^{-3}$) | 0.714 |

The experimental conditions used to perform the $H_2S$ capture using ZnO sorbents are listed in Table 3. In the test bench, a mixture of fuel gas was fed through the ZnO-bed reactor once the system was heated via a Nabeterm muffle furnace. The temperature was fixed between 450 and 600 °C in order to hold the experimental assessments at similar thermal conditions used for the desulfurization stage during the HGC stage. A type K thermocouple was placed inside the reactor in order to measure the internal temperature variations. Likewise, mass flow controllers and a Bronkhorst EL-Flow were connected to control the gas supply, while the data acquisition module/data logger was obtained through Flow-bus communication protocol. To facilitate the gas mixture composition setup, the gas flow control was operated through a designed and customized web server developed using the LabVIEW software. Accordingly, the GHSV was established at 25,000 and 50,000 h$^{-1}$ for all experimental tests by maintaining a constant total flow. The layout of the experimental array can also be seen in Figure 1.

**Table 3.** Sorbent experimental setup using syngas.

| Experimental Conditions | Ranges |
|---|---|
| Sorbent (g) | 0.5–0.25 |
| T (°C) | 450–600 |
| P (bar) | 0.95–1.05 |
| GHSV ($h^{-1}$) | 25,000–50,000 |
| $C_{H_2S}$ (ppmv) | 260 |
| BL (cm) | 0.8–1.5 |
| Bed L/D index | 1–1.9 |
| Particle size (mm) | 1.5–3.0 |
| Total flow (NmL $min^{-1}$) | 305 ± 1 |

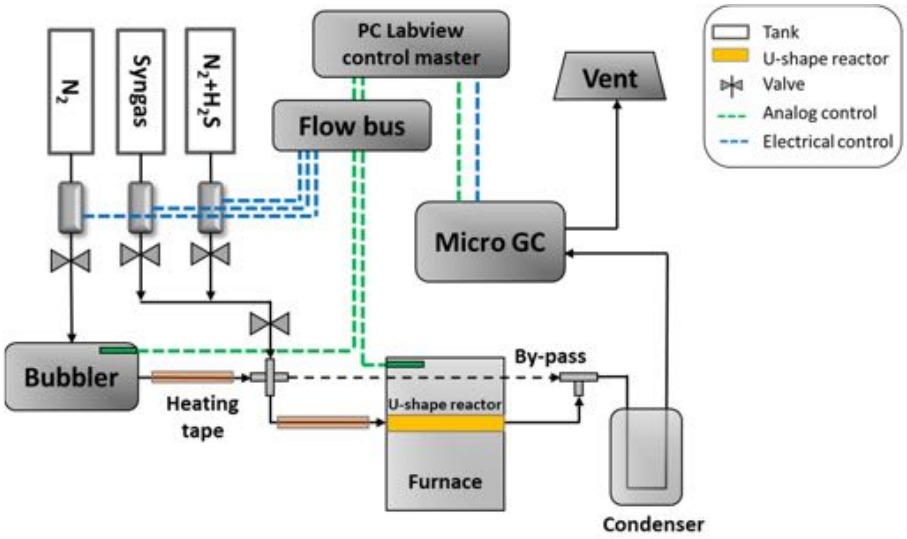


**Figure 1.** The layout of the experimental setup for the adsorption analysis.

The syngas tank has the following composition, 53.9% $H_2$, 29% CO, 14.1 % $CO_2$, and 3% $CH_4$. The syngas was humidified with 20% steam using a cylindrical bubbler heated using a hot-plate magnetic stirrer (Heidolph MR Hei-Tec., Schwabach, Germany). In the same way, pipelines near the furnace inlet were heated in order to maintain the humidified gas flow and to avoid steam condensation. In addition, 260 ppmv of $H_2S$ was supplied to evaluate the desulfurization reaction of ZnO sorbents. An inert gas $N_2$ flow, as a gas carrier, fed both steam and $H_2S$. The total flow rate used in the experimental system was 305 NmL $min^{-1}$.

The gas composition measurement in the outlet of the quartz reactor was carried out with an accuracy of around 1% by using a Micro Gas Chromatograph analyzer model 990 Agilent (Micro-GC) equipped with three column types using carrier gases He and Ar (Molsieve 5Å, CP-Sil 5 CB, and PoraPLOT Q) and the Agilent Openlab software. Before allowing the humidified gas flow to pass through the Micro-GC analyzer, a thermostatic bath (Polyscience 6L) was used to cool down the gas flow and to condensate the excess steam. The steam cooling before gas composition analysis in the Micro-CG was conducted to condense and avoid water excesses in the chromatograph analyzer.

Before starting with the experimental assessments, calibration tests of sensors, actuators, and flow gas control were followed to guarantee reliable measurements. The calibration of the Micro-GC analyzer was also conducted to validate the entire experimentation. In addition, three procedures were always considered before each test: (i) leakage control at junction points, valves, connectors, etc.; (ii) the sulphur loading of the pipeline system until saturation, since tubes can also adsorb $H_2S$; (iii) $N_2$ feeding to suspend or finish a test to facilitate ongoing modifications as well as the shutdown of the whole system. Each experiment had a reference measurement, where the reactor was bypassed in order to

calibrate the system. Additionally, all tests started from steady-state conditions to obtain comparative and reliable results. The equilibrium reaction module of the HSC Chemistry software (version 6, Chemistry Software, Houston, TX, USA) was used to determine the spontaneous and exothermic features ($\Delta G^0 < 0$, $\Delta H^0 < 0$) for the heterogeneous reaction of ZnO and $H_2S$ at different temperatures (450 and 600 °C). In addition, the experimental values were analyzed and simulated by several softwares such as OriginPro (version 2018, OriginLab Corporation, Northampton, MA, USA), Microsoft® Excel® (version 365, Microsoft Corporation, Santa Rosa, CA, USA) and MATLAB (version R2022b, The MathWorks Inc., Natick, MA, USA), using the linearized deactivation kinetic model and nonlinear model fitting. Consequently, adsorption parameters were calculated and their effects on the adsorption process were analyzed.

Considering our previous work consisted of the $H_2S$ uptake using $N_2$ as the carrier with dry and wet conditions [21], it is important to highlight the novelty of the current work. In this case, this investigation evaluated the wet desulfurization reaction at a laboratory scale using similar conditions found in a related industry. Likewise, the insight into the thermodynamic behavior and the kinetic deactivation model at high temperatures was an essential part of this work in order to understand the main thermochemical phenomena that occur during the desulfurization reaction.

## 3. Results and Discussion

### *3.1. Theoretical Approach of the Kinetic Deactivation Model*

In the literature, several models based on unreacted shrinking core or adsorption isotherms have been used to explain the adsorption of contaminants from a gas flow within a pseudo-steady reactor [26]. However, deactivation models often fit better for different pollutant uptakes, including the desulfurization reaction using ZnO sorbents [14,15,17–19,21,22,26,27]. An activation model considers isothermal conditions, external mass-transfer limitations, and the presence of internal diffusion resistances. In this way, it is evident that the physical properties and the functionality of sorbent can affect the adsorption. Thus, a deactivation kinetic model should follow some assumptions concerning the particles and the reactor, which are required to formulate a mathematical interpretation. The model should assume an exponential decrease in the active particle surface, represented through a first-order equation. In addition, regarding the bed reactor, it is necessary to accept a constant gas flow and pseudo-steady state within the bed reactor [26].

Based on the above considerations and assuming that the sorbent deactivation is a first-order equation (n = 1) and zero-order for $H_2S$ concentration (m = 0) [15,22], the deactivation model can be expressed as Equation (1) and integrating with respect to time as Equation (2):

$$\frac{da}{dt} = -k_d\, C_A^m a^n = k_d\, a \tag{1}$$

$$a = a_0\, exp[-k_d\, t] \tag{2}$$

where $da/dt$ is the change rate of adsorbent activity, $k_d$ is the deactivation rate constant ($h^{-1}$), $C_A$ is the $H_2S$ concentration in the gas phase, $a$ is the solid active sites, and $a_0$ is the activity of the solid reactant at the beginning of the sulfidation. Considering the pseudo-steady state conditions for the previous expression, it leads Equation (3) to be expressed as [15,22]:

$$-\dot{V}_g \frac{dC_A}{dm_{ads}} - k_s^*\, C_A\, a = 0 \tag{3}$$

where $\dot{V}_g$ is the total gas flow rate (L $h^{-1}$), $m_{ads}$ is the adsorbent weight (g), and $k_s$* is the initial adsorption rate constant. Assuming that $a_0$ is equal to one at time zero, integrating Equation (3), it is possible to express Equation (4) as:

$$\left(\frac{C_A}{C_{A0}}\right) = exp\left[-\frac{k_s^* m_{ads}}{\dot{V}_g}\ exp(-k_d t)\right] \tag{4}$$

where $C_A$ and $C_{A0}$ are the outlet and inlet $H_2S$ concentrations, respectively. The deactivation model at time zero is represented by Equation (4), and as a consequence of its linearization (Equation (5)), $k_d$ and $k_s$* can be determined by plotting the left side of that equation as a function of time:

$$ln\ (ln\ (\frac{C_{A0}}{C_A}\ )) = ln\ (\frac{k_s^* m_{ads}}{\dot{V}_g}) - k_d t \quad (5)$$

Figure 2 shows the layout of the concentration profile change as a function of the distance from the inlet of the reactor and processing time in a fixed bed reactor for the flow containing a targeted adsorbate (e.g., $H_2S$). As the flow goes forward along the distance of the fixed-bed reactor, a mobile concentration gradient is observed between saturated and absorbate-free adsorbents, known as the mass transfer zone (MTZ). This MTZ leaves an equilibrium zone characterized by a stationary region where adsorbents are completely saturated. This equilibrium region is defined from the inlet to an almost saturated reactor distance ($L_s$). On the contrary, the breakthrough length ($L_b$) is considered to be the starting point of the unused zone, at which the bed is still pristine (breakthrough point). Thus, the site delimited between both $L_s$ and $L_b$ is MTZ, where only the adsorption reaction occurs.

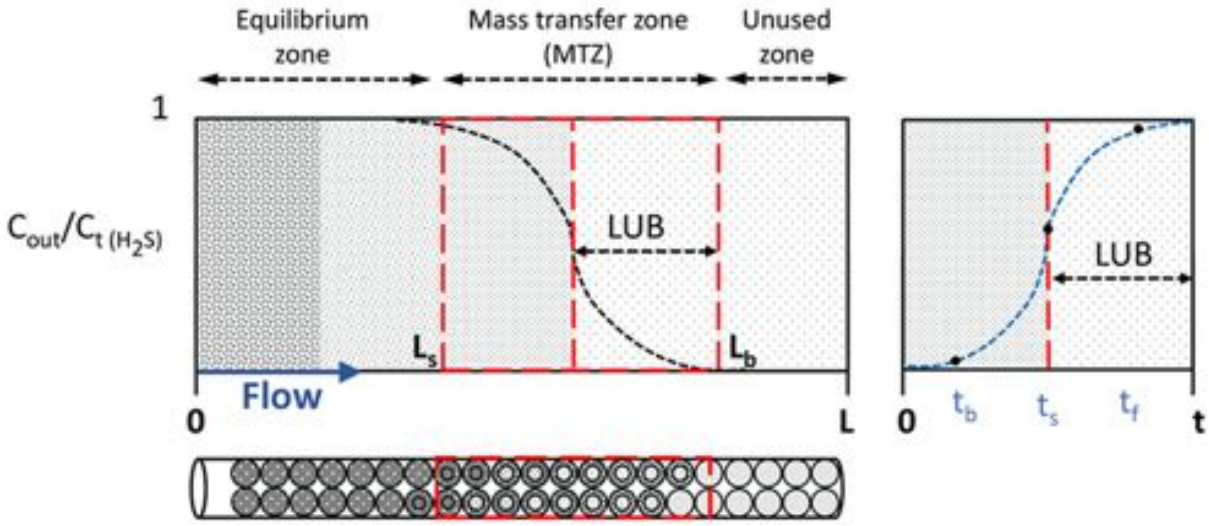


**Figure 2.** Wavefront of the mass-transfer breakthrough curve through an adsorption bed of length L using a starting $H_2S$ concentration ($C_{H_2S}$). $L_s$ and $L_b$ correspond to the saturated and breakthrough length, respectively, while $t_b$, $t_s$, and $t_e$ are associated with breakthrough, stoichiometric, and equilibrium time, respectively.

Since laying down the beginning and the end of MTZ is seldom an immediate determination, a suitable strategy suggests that $L_b$ and $L_s$ are defined as having concentration ratios of 0.05 and 0.95, respectively. An analogous analysis could be proposed for breakthrough ($t_b$) and equilibrium ($t_e$) time. Before $t_b$, the adsorbate concentration is usually less than 5%, leading to discontinued adsorption; when exceeding this threshold, the adsorption occurs and the adsorbent becomes saturated when the completed bed reaches 95%. On the right side of Figure 2, a graphical representation is shown of the concentration change as a function of time in the MTZ with the formation of a typical S-shape curve (breakthrough curve). This type of curve indicates that the system is subjected to different diffusive conditions, such as the formation of an $H_2S$ concentration gradient, along with diffusional resistances of bulk and particle pores and adsorption kinetic processes [22].

Based on previous statements, some parameters have been estimated by fitting experimental results, such as the stoichiometric time ($t_s$), the saturation velocity ($v_s$), and the length of the unused bed (LUB). In fact, knowing the value of $t_s$, the experimental value of $t_b$, and LB, it has been possible to calculate by using expressions (6) and (7) $v_s$ and *LUB*, respectively, which are intrinsic characteristics of the process regardless of the LB value. Moreover, by using expression (8) it has been possible to estimate the length bed ($LB_{est}$)

for each defined breakthrough time, as successively shown. In particular, $t_s$ occurs when the ongoing $H_2S$ concentration reaches half of that concentration at the inlet, meaning that the MTZ is divided into two identical fractions if it is assumed that MTZ = 2LUB. At the same time, $t_b$ is related to the breakthrough concentration, which is established as the initial concentration adsorbed (between 0.5 and 5%). In this investigation, the limit concentration is selected as 2 ppmv (about 0.8% of 260 ppmv), since it is well-known and also supported by related literature that this value is near the maximum allowable concentration of $H_2S$ in the SOFC unit.

$$LUB = \text{LB}\ (1 - \frac{t_b}{t_s}) \tag{6}$$

$$v_s = \frac{\text{LB}}{t_s} \tag{7}$$

$$\text{LB}_{\text{est}} = t_b v_s + LUB \tag{8}$$

Finally, a determining parameter that is useful to select a proper sorbent regarding the desulfurizing performance is the sorbent capacity (SC) in $\left[\frac{g\ sulphur}{100g\ sorbent}\right]$. Equation (9) describes the sulphur adsorbed per mass unit of the used adsorbent material [15]. From this expression, $C_{in}$ and $C_{out}$ correspond to the outlet and inlet $H_2S$ concentrations (ppmv), respectively; $M_S$ is the molar mass of sulphur (32 g $mol^{-1}$); $V_{mol}$ is the molar volume in L $mol^{-1}$; and $t$ is time (h). It is worthwhile to mention that considering the specific time and concentration, it is possible to determine the breakthrough and equilibrium sorbent capacity.

$$\text{SC} = \text{GHSV}\ \left(\frac{M_s}{V_{mol}}\int_0^t C_{in} - C_{out}dt\right) 1 \times 10^{-4} \tag{9}$$

### *3.2. Analysis of the $H_2S$ Adsorption Using ZnO in the Presence of Syngas*

#### 3.2.1. Breakthrough Curves for the Hydrogen Sulphide Adsorption

An assessment of $H_2S$ capture using ZnO sorbents was carried out to clean the syngas flow fed in a thermal range between 450 and 600 °C with an increasing step of 50 °C. Two experimental campaigns were undertaken by varying the LB value between 0.8 and 1.5, causing changes in both the internal diffusive resistance and adsorption kinetics. According to previous LB values and by constantly maintaining the total gas flow at 305 NmL $min^{-1}$, the GHSV was defined as 50,000 and 25,000 $h^{-1}$, respectively. Figure 3 shows the breakthrough curves for the $H_2S$ capture in terms of the time at temperatures between 450 and 600 °C and GHSV, leaving the total flow constant and changing the LB value. The experimentation took more than 3 h to reach the $t_b$ when the sorbent showed $H_2S$ adsorption around 2 ppmv. For the desulfurization reaction (Equation (10)), the values of $\Delta H^0$ and $\Delta G^0$ were calculated using data at 25 °C and Kirchhoff equations. Thermodynamic parameters used for the previous calculation are summarized in Table 4.

$$ZnO_{(s)} + H_2S_{(g)} \leftrightarrow ZnS_{(s)} + H_2O_{(g)} \tag{10}$$

**Table 4.** Thermodynamic parameters for the hydrogen sulphide adsorption.

| Specie | $\Delta H^0_{f,\,25\,^\circ C}$ (kJmol$^{-1}$) | $S^0_{25^\circ C}$ (Jmol$^{-1}$K$^{-1}$) | $C_p(T)$ (J mol$^{-1}$·K$^{-1}$) |
|---|---|---|---|
| $H_2O$ | −241.8 | 188.7 | $23.0 + 1.28 \times 10^{-5}$ T |
| $H_2S$ | −20.6 | 205 | $29.9 + 1.55 \times 10^{-5}$ T |
| ZnO | −348 | 43.6 | 40.2 |
| ZnS | −202 | 57.7 | 53.6 |

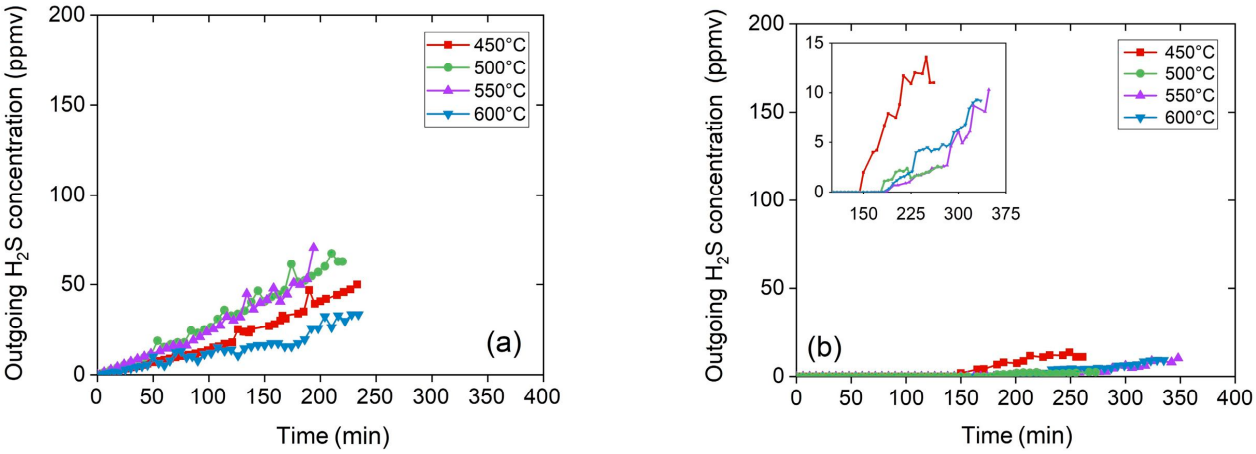


**Figure 3.** Outgoing $H_2S$ concentration vs. time plot at different temperatures (450, 500, 550, and 600 °C) considering a GHSV equal to (**a**) 50,000 $h^{-1}$ and (**b**) 25,000 $h^{-1}$ considering a gas flow of 305 NmL $min^{-1}$.

By applying the Kirchhoff Equations (11) and (12), it is possible to calculate the thermodynamic constant value for the adsorption reaction as a function of temperature, as shown in Equation (13). In agreement with values from the literature [28,29], the $K_p$ value at 300 °C is $5.9 \times 10^6$, while at 25 and 600 °C the values are $1.3 \times 10^{13}$ and $3 \times 10^4$, respectively. The average values of $\Delta G$ and $\Delta H$ in the studied temperature range are −74.5 kJ $mol^{-1}$ and −72.4 kJ $mol^{-1}$, respectively. The calculations were also confirmed by using the HSC Chemistry 6 software.

$$\Delta H_f^o(T) = \Delta H_f^o(298.15) + \int_{298.15}^{T} C_p(T)dT \quad (11)$$

$$S^o(T) = S^o(298.15) + \int_{298.15}^{T} \frac{C_p(T)}{T}dT \quad (12)$$

$$K_p(T) = \exp\left[\frac{9321}{T} - 1.62 \times 10^{-4}T + 9.62 \times 10^{-1}\ln(T) - 6.69\right] \quad (13)$$

Figure 3a,b and Table 5 describe the breakthrough curves during the $H_2S$ adsorption using ZnO in the same temperature range at 50,000 and 25,000 $h^{-1}$ and LB sizing. Different effects changing the GHSV are observed in Figure 3a,b. This variation is also highlighted in the inlet of Figure 3b, where the first stage of the $H_2S$ saturation process takes more time to be evident. The modeling of breakthrough curves calculates the kinetic parameters ($k_d$ and $k_s$*) by linearizing the deactivation equation (Equation (5)) and plotting the left members in the function of time. Figure 4a,c show the plot of the linearized deactivation kinetic model between 450 and 600 °C for 50,000 and 25,000 $h^{-1}$, respectively.

Based on $k_d$ and $k_s$*, breakthrough curves were suitably fitted by reaching a good adjustment ($R^2 > 0.90$), as shown in Figure 4b,d. In Figure 4, all the fitting curves have the characteristic S-shape, even if they are not completely shown on graphs, for better readability. The fitting of the breakthrough curves lead to the LB reactor sizing, as well as evaluating the reactor performance and understanding the kinetic and mass-transfer phenomena of the adsorption process. Furthermore, another influencing parameter on the adsorption process is GHSV.

**Table 5.** Outputs from breakthrough curves, kinetic constant, and sizing of LB.

| LB (cm) | GHSV ($h^{-1}$) | T (°C) | ln ($k_s$ $m_{ads}$ $\dot{V}_g^{-1}$) | $k_s$* (L $g^{-1}h^{-1}$) | $k_d$ ($h^{-1}$) | $R^2$ | $t_b$ (min) | $t_s$ (min) | $SC_b$ | $SC_e$ | $v_s$ (cm $min^{-1}$) | LUB (cm) | MTZ (cm) |
|---|---|---|---|---|---|---|---|---|---|---|---|---|---|
| 1.5 | 25,000 | 600 | 2.55 | 1503 | 0.229 | 0.88 | 250 | 875 | 5.1 | 18 | $1.71 \times 10^{-3}$ | 1.07 | 2.14 |
| | | 550 | 2.60 | 1490 | 0.245 | 0.97 | 250 | 840 | 5.1 | 19 | $1.79 \times 10^{-3}$ | 1.07 | 2.14 |
| | | 450 | 2.30 | 969 | 0.320 | 0.92 | 131 | 591 | 2.7 | 15 | $2.54 \times 10^{-3}$ | 1.17 | 2.33 |
| 0.8 | 50,000 | 600 | 1.66 | 1235 | 0.242 | 0.93 | 22 | 611 | 1.2 | 24 | $1.31 \times 10^{-3}$ | 0.77 | 1.54 |
| | | 550 | 1.37 | 871 | 0.261 | 0.93 | 3 | 541 | 0.12 | 19 | $1.47 \times 10^{-3}$ | 0.80 | 1.59 |
| | | 500 | 1.28 | 796 | 0.271 | 0.96 | 2 | 511 | 0.08 | 19 | $1.56 \times 10^{-3}$ | 0.80 | 1.59 |
| | | 450 | 1.35 | 750 | 0.223 | 0.97 | 1 | 605 | 0.05 | 24 | $1.32 \times 10^{-3}$ | 0.79 | 1.57 |

$k_s$* (initial adsorption rate constant expressed in L $g^{-1}$ $h^{-1}$). $SC_b$, $SC_e$ (g sulphur per 100 g sorbent).

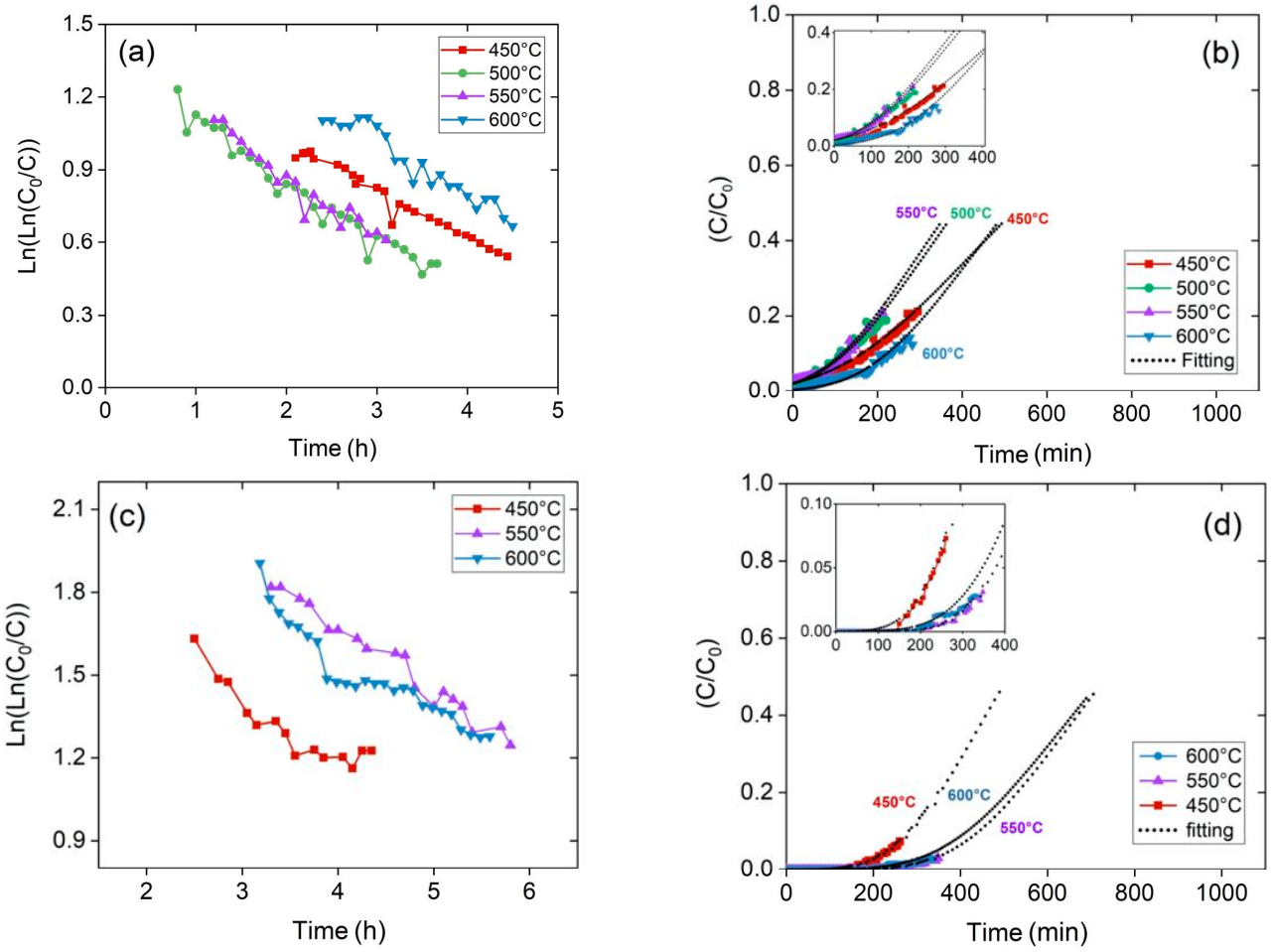


**Figure 4.** Linearized deactivation kinetic model ln(ln($C_0$/C)) vs. time and breakthrough curves fitting (**a**,**b**) calculated by using GHSV equal to 50,000 (upper) at 450, 500, 550, and 600 °C and linearized deactivation kinetic model ln(ln($C_0$/C)) vs. time and breakthrough curves fitting (**c**,**d**) calculated by using GHSV equal to 25,000 $h^{-1}$ (lower) at 450, 550, and 600 °C.

The variation of GHSV caused by changing the volume's bed or flow rate generates that the contact time between the adsorbate and the bed of ZnO sorbent can vary. When bed size is underestimated, small LUB and MTZ values, and accordingly small $t_b$ and $t_s$, are obtained, which is equivalent to suggesting a faster mass-transfer and adsorption kinetics process. On the contrary, these diffusive processes can be determined by global resistance due to the size particle effect, such as intraparticle mass transfer resistance [30]. At a typical industrial scale for the gas cleaning process, particle sizes higher than 1 mm

diameter are employed, similar to the particles used in this work. In that way, only external mass transfer could be omitted, while internal resistances stand out (diffusional resistances related to intraparticle mass transfer). Concerning the effect of intraparticle resistance, it can be lowered as particle size decreases; however, pressure drops are a critical phenomenon that can take place. Therefore, a suitable compromise should be proposed by considering small particle sizes, at which the intraparticle resistances are reasonably low, but at the same time, the risk of pressure drops is avoided.

From experimentation, the $t_b$ and Sorption capacity at breakthrough ($SC_b$) values are determined and reported in Table 5. Following the modeling of the deactivation model, along with experimental values, $k_s$*, $k_d$, sorption capacity at equilibrium ($SC_e$), $t_s$, and $v_s$ were obtained. Subsequently, by using Equations (6) and (7), LUB and MTZ are calculated, as shown in Table 5. Considering Equations (6) and (7), it is possible to determine LUB and MTZ using the experimental LB. However, it is widely known that scaling up requires that the whole LB is greater than the MTZ; otherwise, the length of the used bed will be insignificant and an unstable mass-transfer zone can occur [21,22]. According to Table 5, MTZ is greater than LB in all cases; nonetheless, it can be used to understand the adsorption results in the reactor [21,22].

Regarding the analysis of the MTZ, short LB (consequently high GHSV) causes a decrease both in utilization efficiency and $SC_b$. Thus, the direct effect of reducing LB in half is unstable mass transfer conditions. Hence, when it works with lower GHSV conditions, the thermodynamic effects start to have an influence, while with higher GHSV conditions, the kinetic effects are more relevant. Based on our results, the tests at 25,000 $h^{-1}$ are also influenced by thermodynamic phenomena, unlike tests at 50,000 $h^{-1}$. In the literature, it is well known that a temperature increase favors mass-transfer processes (as observed in our results), showing an increase in $SC_b$ as temperature rises. However, on the other side, exothermic reactions are thermodynamically unfavorable as temperature increases.

Regarding $SC_b$, the best performance for ZnO sorbents at 25,000 and 50,000 $h^{-1}$ was achieved between 550 °C and 600 °C capturing about 5.1 g of sulphur from 100 g of adsorbent. Further, it is necessary to mention that the test at 450 °C and 50,000 $h^{-1}$ shows anomalous behavior, probably due to unexpected experimental variations, while the test at 500 °C and 25,000 $h^{-1}$ shows two different trends, and it has not been taken into consideration. Despite the previous anomalous tests, the following analyses and considerations on collected data consider all tests performed, including those produced in earlier work, to arrive at a coherent and consistent conclusion.

Based on the previous analyses and kinetic parameter calculations, we estimate the LB ($LB_{est}$) value, at which the ZnO bed-fixed reactor can work efficiently for an extended period. In this case, once the value of $v_s$ is known and estimated from the modeling of experimental results, it is possible to estimate the $LB_{est}$ using the desired $t_b$ (for example, $t_b$ = 1000 h). In Table 6, the $LB_{est}$ necessary to work for a long period without observing $H_2S$ saturation was estimated. This estimation was performed using Equation (8) and by considering the $v_s$ obtained from the current experimental conditions and those taken from [21]. From the obtained results herein using 260–400 $H_2S$ ppm, it is evident that by using an $LB_{est}$ in a range of about 100–130 cm, it is possible to have a bed of sorbent with a capacity to work about 1000 h. These estimations are in agreement with the previous analysis, where an increase in temperature, in general, favors the desulfurization reaction. In particular, when GHSV is changed by increasing the gas flow, the relative velocity of the gas flow rises with respect to the fixed bed and LB significantly increases. Thus, this is a critical parameter to size the LB. In fact, in this test, changing the GHSV (by changing gas flow) to 40,000 $h^{-1}$ at 550 °C causes the LB to be proportionally increased. Finally, considering unexpected variations, the test at 50,000 $h^{-1}$ and 450 °C confirmed an anomalous result since it was expected to be an $LB_{est}$ larger than others at the same GHSV and higher temperatures.

**Table 6.** Estimation of the BL for a breakthrough time of 1000 h by analyzing the operative conditions and outcomes obtained in our current investigation and those found in the literature [21].

| Concentration ($H_2S$ ppm) | T (°C) | GHSV ($h^{-1}$) | $v_s$ (cm $h^{-1}$) | $LB_{est}$ for $t_b$ of 1000 h (cm) | Reference |
|---|---|---|---|---|---|
| 260 | 600 | 25,000 | 0.100 | 101 | This work |
| | 550 | 25,000 | 0.107 | 108 | |
| | 450 | 25,000 | 0.152 | 153 | |
| | 600 | 50,000 | 0.090 | 91 | |
| | 550 | 50,000 | 0.102 | 103 | |
| | 500 | 50,000 | 0.106 | 107 | |
| | 450 | 50,000 | 0.089 | 90 | |
| 400 | 600 | 50,000 | 0.094 | 95 | [21] |
| | 550 | 40,000 | 0.180 | 180 | |
| | 600 | 25,000 | 0.097 | 98 | |
| | 550 | 25,000 | 0.089 | 90 | |
| | 500 | 25,000 | 0.107 | 108 | |
| | 450 | 25,000 | 0.129 | 130 | |
| | 400 | 25,000 | 0.133 | 134 | |

#### 3.2.2. Gas Composition Analysis during ZnO-Based Sorbent Performance

Since assessments were performed using a mixture of biogas, other reactions (WGS, methane reforming, etc.) could happen. Thus, ZnO adsorbents were evaluated under wet conditions for assessing two cases: gas flow (i) through and (ii) bypassing the furnace. These assessments were conducted at 600 °C, while the furnace by-passing condition was performed at room temperature. Given that no thermochemical reaction was expected, the by-passing condition was considered to be the base measurement. All the measurements were carried out using an Agilent Micro-GC 990 gas chromatograph analyzer, which has been described above. In this study, the bed weight was increased to 15 g, while the syngas flow gas remained unchanged at 305 NmL $min^{-1}$. The $H_2S$ concentration was also increased to 400 ppmv, while the steam addition varied from 0% to 20%. Table 7 shows the variation of the gas composition with and without steam presence when the gas passes through the reactor containing ZnO adsorbents. In these results, it is observed that, at high temperatures (600 °C), there is an increase in the hydrogen content as steam increases due to the endothermic methane reforming and the WGS reaction (Equations (14) and (15)). Regarding $H_2S$ interactions with syngas components (CO and $CO_2$), thermodynamic analysis from the literature and HSC 6 Chemistry have been indicated to be more favorable conditions for Equation (16) than for Equation (17), as temperature increases [22]; however, in this investigation, COS was not observed in the chromatography results during the HGC process.

$$CH_4 + H_2O \rightleftharpoons CO + 3H_2 \quad (14)$$

$$CO + H_2O \rightleftharpoons CO_2 + H_2 \quad (15)$$

$$CO_2 + H_2S \rightleftharpoons COS + H_2O \quad (16)$$

$$CO + H_2S \rightleftharpoons COS + H_2 \quad (17)$$

**Table 7.** Gas concentration variation considering the gas flow through the furnace at 600 °C with and without steam. Measurements had a standard deviation inferior to 0.4.

| | | Gas Composition (%) | | | |
|---|---|---|---|---|---|
| **Condition** | **Steam (%)** | **$H_2$** | **CO** | **$CO_2$** | **$CH_4$** |
| By-passing | - | 54.8 | 29.6 | 12.5 | 3.1 |
| Furnace | 0 | 51.4 | 35.9 | 9.5 | 3.2 |
| Furnace * | 20 | 56.7 | 23.7 | 16.6 | 2.9 |

* The steam was not included in the micro-GC analysis since it was removed by a condenser upstream.

To highlight the effect of the ZnO sorbent on the methane reforming and WGS reaction (Equations (14) and (15)), the same experimentation with the same operative conditions and without ZnO sorbents were performed. Table 8 shows the variation of the gas composition when the gas passes and bypasses the furnace using 20 and 0% of steam without the presence of the adsorbent material in the reactor. Considering the sorbent absence, the variation of the gas composition remains constant. These results confirmed that the material could be used for HGC capturing H2S from the fuel stream, and the presence of this material at high temperatures can facilitate alternate reactions such as methane reforming and WGS. Additionally, it is worth mentioning that during all experimental campaigns at high temperatures (up to 600 °C), sorbent remained physically stable with no evidence of ZnO volatilization.

**Table 8.** Results of blank tests with the following gas composition variation considering the gas flow through the furnace at 600 °C with and without steam. This assessment was performed without sorbent inside the quartz reactor and all results had a standard deviation inferior to 0.4%.

| | | Gas Composition | | | |
|---|---|---|---|---|---|
| **Condition** | **Steam (%)** | **$H_2$** | **$CH_4$** | **CO** | **$CO_2$** |
| By-passing | - | 54.7 | 29.4 | 12.8 | 3.1 |
| Furnace | 0 | 54.4 | 29.4 | 13.1 | 3.1 |
| Furnace * | 20 | 54.7 | 29.4 | 12.8 | 3.1 |

* The steam was not included in the micro-GC analysis since it was removed by a condenser upstream.

### *3.3. Modeling of the Breakthrough Curve using the Kinetic Deactivation Model*

The characterization of the adsorption process as operative process conditions vary is achieved by the understanding and determination of the breakthrough curves. This type of study leads to the sizing of fixed bed reactors. In this section, we consider the breakthrough curves and the analyses of the influencing parameters on the linearized kinetic deactivation model. To carry out those analyses, Equation (5) is rewritten as Equation (18):

$$ln\left(ln\left(\frac{C_{A0}}{C_A}\right)\right) = ln\,(\mathrm{P2}) - \mathrm{P1}\cdot t \tag{18}$$

Concerning the theoretical values (P1 and P2) from the right members of the deactivation model in the linearized form of Equation (5), the former value is related to $k_d$ expressed in $h^{-1}$, while the latter value corresponds to the dimensionless relationship among $k_s$*, $m_{ads}$, and $\dot{V}_g$. Figure 5 shows different simulated conditions to determine and understand the influence of the kinetic parameters on the shape of the breakthrough curve (slope, $t_b$, $t_s$, $t_e$, etc.).

Figure 5a shows the influence of P2 on the breakthrough curve while P1 is maintained unchanged. As P2 increases, it can be observed that the breakthrough curve shifts towards the right side, suggesting that MTZ remains unchanged. In other words, P2 does not affect the shape of the breakthrough curve; while maintaining a fixed LB, $t_b$ and $t_s$ increase and the $v_s$ becomes slower. Furthermore, Figure 5b shows the effect of P1 on the breakthrough curve, while maintaining a constant value of P2. By decreasing only P1, the front wave shifts towards the left side and the curve shape changes. In consequence, MTZ becomes smaller as much as P1 does. That means, by maintaining a fixed LB, $t_b$ and $t_s$ decrease and the $v_s$ is higher.

Figure 5c presents a simulation of breakthrough curves performed by changing the $H_2S$ concentration from 410 to 260 ppmv, while the other operative conditions are unchanged. This Figure indicates a slight modification in the breakthrough curve shape, suggesting a faster deactivation process for a flow with a higher concentration of $H_2S$. This behavior is also confirmed with higher $t_b$. In the case of $t_s$ (in the middle of both curves), the $H_2S$ concentration remains virtually unchanged, given that even if $t_b$ increases, the MTZ shrinks when lowering the concentration.

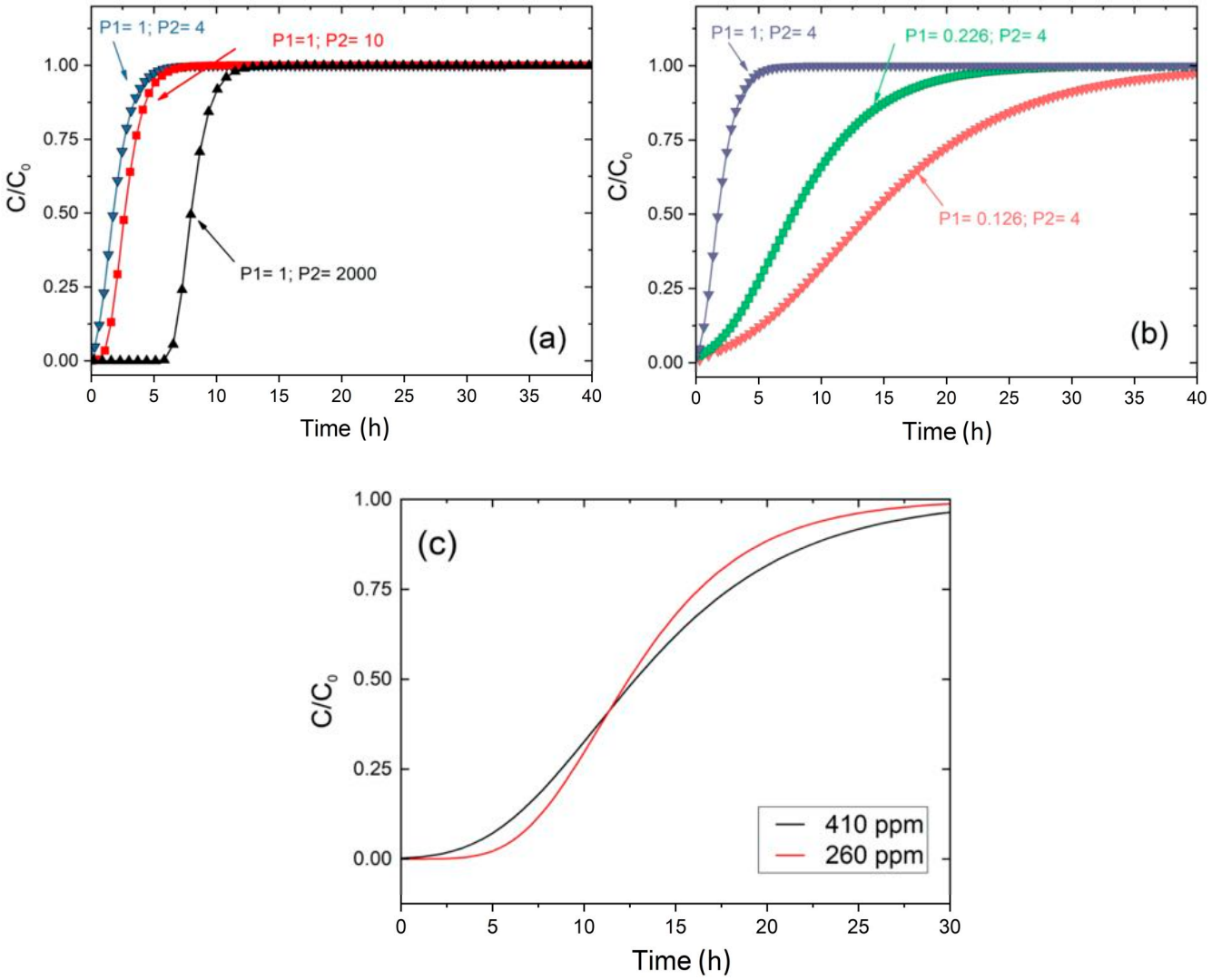


**Figure 5.** Modeling of breakthrough curves based on the deactivation model in linearized form changing the kinetic parameters noted by P1 and P2: (**a**) P1 remains constant, while the P2 value varies; (**b**) P2 remains constant, while the P1 value varies; (**c**) simulation of breakthrough curves at 25,000 $h^{-1}$ GHSV, 600 °C as temperature, and LB equal to 1.5 cm for two different $H_2S$ concentrations used in present tests.

Table 9 shows P1, P2, $v_s$, and $k_s$* for the experimental results obtained in this investigation and those found in [22]. Some parameters presented in [22] were recalculated to complement our current analysis. By analyzing the results gathered in Table 9, it is worth highlighting that if GHSV is increased by halving the LB, the $v_s$ can remain unchanged because it is the ratio between the BL and $t_s$. While if GHSV is increased by increasing the gas flow, $t_s$ decreases and $v_s$ increases. For instance, by doubling GHSV because of the halving of LB, $t_s$ will also be halved and the $v_s$ remains unchanged; but if GHSV is doubled just by the gas flow (with the same LB), $t_s$ will be halved and $v_s$ will be doubled. In conclusion, the most influence on the $v_s$ is the relative velocity between gas flow and sorbent.

When operative conditions are modified, other relationships have been observed related to $k_d$ and $k_s$*. In the temperature variation, $k_s$* is, in general, directly affected, while $k_d$ has an inverse change. On the contrary, when GHSV varies, it causes a direct and inverse effect on $k_d$ and $k_s$*, respectively. However, the concentration changes show an inverse impact on both $k_d$ and $k_s$*.

**Table 9.** Kinetic parameters from the fitting of the deactivation model (P1 ($k_d$), P2, $v_s$, and $k_s$*) for experimental results obtained in this investigation and found in [22].

| | P1 | P2 | $k_s$* | $k_s$ | P1 | P2 | $k_s$* | $k_s$ | P1 | P2 | $k_s$* | $k_s$ | P1 | P2 | $k_s$* | $k_s$ |
|---|---|---|---|---|---|---|---|---|---|---|---|---|---|---|---|---|
| | ($h^{-1}$) | | (L $g^{-1}$ $h^{-1}$) | ($s^{-1}$) | ($h^{-1}$) | | (L $g^{-1}$ $h^{-1}$) | ($s^{-1}$) | ($h^{-1}$) | | (L $g^{-1}$ $h^{-1}$) | ($s^{-1}$) | ($h^{-1}$) | | (L $g^{-1}$ $h^{-1}$) | ($s^{-1}$) |
| **$H_2S$ concentration(ppm)** | 410 [21] | | | | | | | | 216 (This work) | | | | | | | |
| **GHSV($h^{-1}$)** / **T (°C)** | **25,000** | | | | **50,000–40,000** | | | | **25,000** | | | | **50,000** | | | |
| 600 | 0.171 | 5.75 | 675 | 0.073 | 0.226 | 2.71 | 636 | 0.069 | 0.229 | 12.81 | 1503 | 0.114 | 0.242 | 5.26 | 1235 | 0.093 |
| 550 | 0.173 | 7.24 | 801 | 0.092 | 0.292 | 4.42 | 784 | 0.090 | 0.245 | 13.46 | 1490 | 0.119 | 0.261 | 3.78 | 837 | 0.067 |
| 500 | 0.184 | 5.05 | 525 | 0.064 | - | - | - | - | - | - | - | - | 0.271 | 3.48 | 780 | 0.063 |
| 450 | 0.206 | 4.06 | 394 | 0.052 | - | - | - | - | 0.32 | 9.97 | 970 | 0.089 | 0.223 | 3.53 | 758 | 0.069 |

$k_s$* (the initial adsorption rate constant expressed in L $g^{-1}$ $h^{-1}$).

### *3.4. Activation Energy and Thermodynamic Parameters of the Adsorption Reaction*

The minimum required energy to achieve the reactant-to-product conversion for a determined reaction is described by $E_a$, where a high or low $E_a$ suggests an accelerated or slowed-down reaction progress. Temperature, $H_2S$ concentration, GHSV, type of sorbent, gas composition, and particle size can affect the kinetic adsorption reaction, requiring the necessary energy to carry out the ZnS occurrence, as shown in Equation (10). Thus, attempting to interpret the phenomenon on $H_2S$ capture, the results from the experimental campaign have been used to calculate both $E_a$ and transition state parameters (Gibbs free energy, enthalpy, and entropy).

To obtain the $E_a$, it is necessary to know the $k_s$* value as a function of temperature and fit experimental data represented through the deactivation model in Equation (5). Following that fitting, it is possible to determine $k_s$* via the intercept calculation. In some studies in the literature [18,31], $k_s$* has been expressed in L $g^{-1}$ $h^{-1}$, (gas flow expressed in L $h^{-1}$ per gram of sorbent) but it can also be expressed in $s^{-1}$ (gas flow expressed in g $s^{-1}$ per gram of sorbent, in which case, $k_s$ has been used as a notation), whose values are also reported in Table 9.

Thus, $k_s$ values are linked to $k_s$* by a proportionality factor that is gas density, which neglecting, for simplicity the slight pressure variation, is a function only of the temperature, that is, $k_s^* = aTk_s$. Therefore, the analysis presented above for $k_s$ is also analogous to $k_s^*$. By using the Arrhenius equation (Equation (19)), $k_s$ can be used in both ways. While using the Eyring–Polanyi equation (Equation (20)) and considering the transition state theory [32–34], it must be expressed in the reciprocal value of time ($s^{-1}$). By using the Arrhenius equation, the apparent activation energy ($E_a$*) (Figure 6b) and $E_a$ (Figure 6a) can be calculated. The Arrhenius equation is written as follows:

$$k_s = Ae^{\frac{-E_a}{RT}} \quad (19)$$

where $A$ and $E_a$ are the frequency factor or pre-exponential coefficient and activation energy (J/mol), respectively; $R$ and $T$ are the molar universal gas constant (8.314 J $mol^{-1}$ $K^{-1}$) and the absolute temperature (K), respectively.

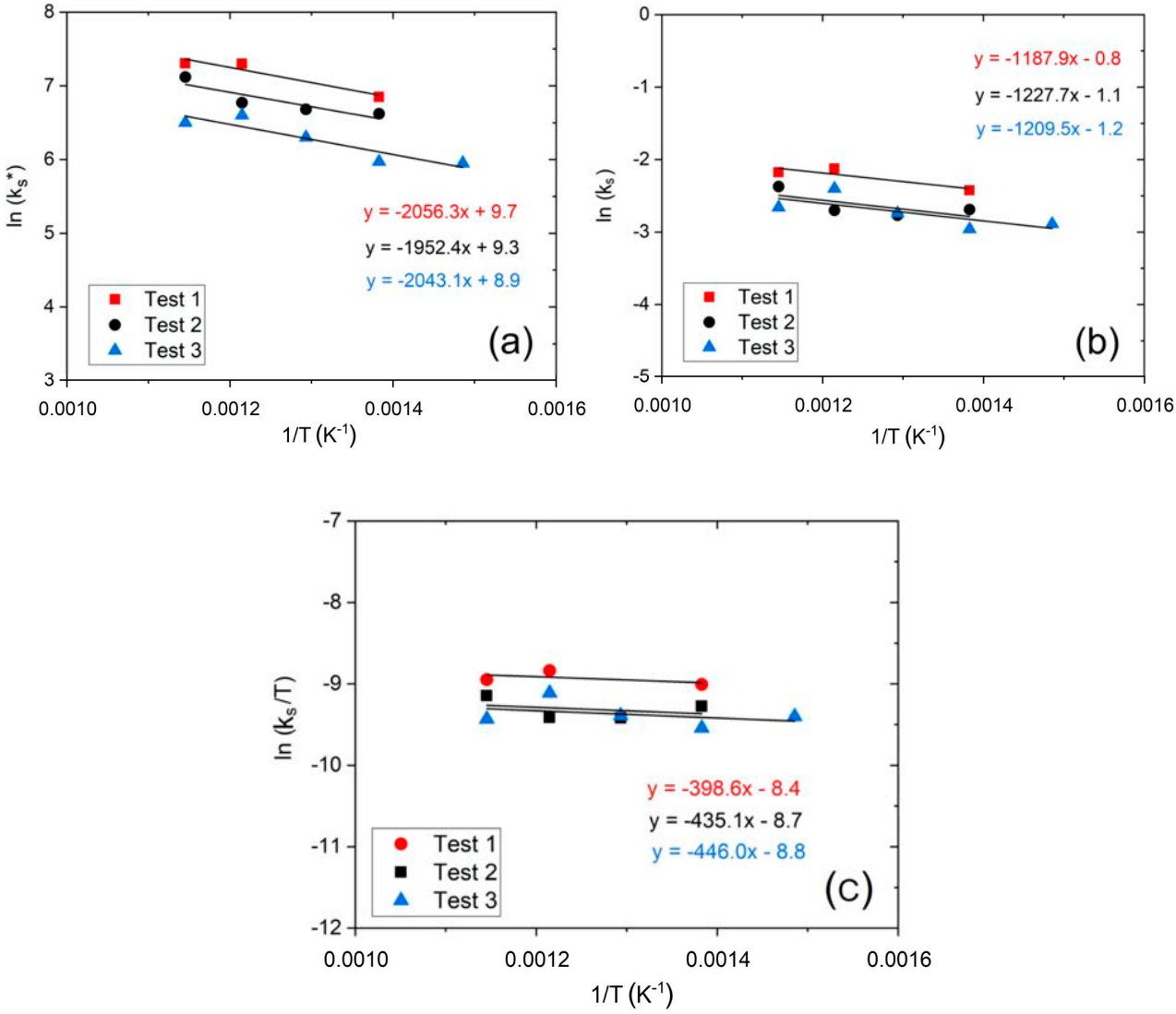


**Figure 6.** Arrhenius plots in terms of (**a**) $k_s^*$ and (**b**) $k_s$; (**c**) the Eyring–Polanyi representation plotting $ln(k_s/T)$ vs. the reciprocal temperature. Test 1 (red circle) corresponds to experimentation using syngas, 1.5 cm LB bed length, and GHSV equal to 50,000 $h^{-1}$; Test 2 (black square) involves the investigation using syngas, 0.8 cm LB, and GHSV equal to 25,000 $h^{-1}$; Test 3 (blue triangle) is associated with humid hydrogen, 1.5 cm LB, and GHSV equal to 25,000 $h^{-1}$.

While the Eyring–Polanyi equation is:

$$k_s = \frac{k_b T}{h}\, exp\left(\frac{-\Delta G^*}{RT}\right) \tag{20}$$

where $\Delta G^*$ is the free energy activation and $\Delta G^* = \Delta H^* - T\Delta S^*$, we have that $\Delta G^*$ is always positive because there is always a barrier to reaction; the $k_s$ is the adsorption rate constant in $s^{-1}$; h and $k_b$ are Plancks ($6.63 \times 10^{-34}$ J s) and Boltzmann ($1.38 \times 10^{-23}$ $JK^{-1}$) constants. By rearranging the Eyring–Polanyi equation and taking logarithms (Equation (21):

$$ln\left(\frac{k_s}{T}\right) = ln\left(\frac{k_b}{h}\right) + \frac{\Delta S^*}{R} - \frac{\Delta H^*}{R}\left(\frac{1}{T}\right) \tag{21}$$

Figure 6 shows the linearized Arrhenius (Figure 6a,b) and Eyring–Polanyi (Figure 6c) equations for the experimental data at different temperatures. The GHSV was varied and each condition was named Tests 1–3 (Test 1 corresponds to experiments using syngas with

1.5 cm LB and GHSV equal to 50,000 $h^{-1}$, Test 2 includes experiments using syngas with 0.8 cm LB and GHSV equal to 25,000 $h^{-1}$, and Test 3 is obtained by using humid hydrogen with 1.5 cm LB and GHSV equal to 25,000 $h^{-1}$ [21]). By plotting *ln($k_s$) or ln($k_s$*)* values for all tests (Test 1, Test 2, and Test 3) as a function of the reciprocal term of temperature, the slope from the linearized Arrhenius expression determines $E_a$ and $E_a$* to be about 10 kJ $mol^{-1}$ and 17 kJ $mol^{-1}$, respectively.

By using the Eyring–Polanyi equation along with Test 1, Test 2 and Test 3, it is also possible to calculate $E_a$ defined in Equation (22). The result is 10.1 kJ $mol^{-1}$. Then, it is possible to state that regardless of the gas composition, the adsorption process is the same for the three tests and proceeds with the same mechanism.

$$E_a = \Delta H^* + RT \tag{22}$$

It is possible to calculate $\Delta H^*$ and $\Delta S^*$ of the transition state by plotting *ln($k_s$/T)* as a function of the reciprocal term of temperature in Kelvin. The Eyring–Polanyi plot was obtained and is reported in Figure 6c. The $\Delta H^*$ and $\Delta S^*$ values for the transition state were calculated for all cases taken into consideration, as shown in Table 10. A positive value of $\Delta H^*$ means that passing from reactants to the transition state heat is required, while a negative value of $\Delta S^*$ means that the degree of disorder of the transition state is lower than that of the reactant.

**Table 10.** Thermodynamic parameters for the transition state.

| $\Delta H^*$ (kJ $mol^{-1}$) | $\Delta S^*$ (kJ $mol^{-1}$ $K^{-1}$) |
|---|---|
| 3.31 | −0.267 |
| 3.62 | −0.270 |
| 3.71 | −0.270 |

As shown in Figure 6b, reporting the trend of *ln($k_s$)* as a function of the reciprocal of the temperature, despite the presence of oscillations, it is possible to observe how the adsorption constant rate increases with increasing temperature. Considering the expression in Equation (23), the increase rate in the used temperature range was determined to be 1.58 $\times 10^{-4}$ $s^{-1}$ $K^{-1}$ as follows:

$$\frac{dk_s}{dT} = \frac{AE_a}{RT^2} e^{-\frac{E_a}{RT}} \tag{23}$$

### *3.5. Kinetic Reactions Parameters and Diffusion Coefficient Determination*

The spherical geometry model is another way to understand the adsorption phenomenon in a geometry similar to realistic conditions. Equation (24) shows the gas concentration rate inside the particle in terms of spherical variables.

$$\frac{dC_p}{dt} = -D\frac{1}{r^2}\frac{d}{dr}\left(\frac{dC_p}{dr} \cdot r^2\right) - k_0 C_p \tag{24}$$

where $D$ is the diffusion coefficient in $m^2/s$, $C_p$ is the gas concentration within the particle in mol $m^{-3}$, $r$ is the spherical coordinate, and $t$ is the time in $s$. Concerning non-steady conditions, a suitable solution for the partial differential equation (Equation (24)) could be obtained by imposing $C_p(r,t) = X(t) \cdot Y(r)$, that is, the variable $C_p$ is decomposed into two variables, such as $t$ or $r$. In this way, the left-hand side of these equations can only be a function of $t$ and the right-hand side is only a function of $r$. In the Supplementary Material S1, Equation (24) in spherical geometry has been mathematical elaborated in order to obtain a $D$ and $k_s$ in terms of spherical geometry. In Equations (25) and (26) can be seen the $D$ and $k_0$:

$$D = \frac{k_s k_d W R^2}{3Q(1-\varepsilon)} \tag{25}$$

$$k_0 = \frac{\pi^2 D}{R^2} - k_d \quad (26)$$

Assuming a particle ratio (R) equal to 1.5 mm and a vacuum degree (ε) of the reactor equal to 0.1, all the hypotheses made upstream have been verified. In Table 11 lists the operative parameters for all experimental conditions from this investigation and the results reported in [21].

**Table 11.** Kinetic reaction parameters and diffusion coefficients using a spherical geometry model.

| | GHSV ($h^{-1}$) | Temp. (°C) | $D$ ($m^2/s$) $1 \times 10^{-10}$ | $\bar{k_0}$ ($s^{-1}$) $1 \times 10^{-3}$ |
|---|---|---|---|---|
| This work | 50,000 | 600 | 2.94 | 1.2 |
| | | 550 | 2.28 | 0.92 |
| | | 500 | 2.20 | 0.89 |
| | | 450 | 2.01 | 0.82 |
| | 25,000 | 600 | 6.78 | 2.90 |
| | | 550 | 7.64 | 3.30 |
| | | 450 | 7.38 | 3.10 |
| [21] | 50,000 | 600 | 2.04 | 0.83 |
| | 40,000 | 550 | 4.3 | 1.80 |
| | 25,000 | 600 | 3.27 | 1.40 |
| | | 550 | 4.16 | 1.80 |
| | | 500 | 3.09 | 1.30 |
| | | 450 | 2.78 | 1.20 |

## 4. Conclusions

The removal of critical contaminants that are downstream of a biofuel conversion SOFC system has led this work to propose the study of the wet desulfurization reaction using realistic operative conditions regarding temperature and gas composition. Commercial zinc oxide was used as a material adsorbent in a fixed-bed reactor in a thermal range between 450 and 600 °C and a gas mixture containing wet syngas and $H_2S$ as a contaminant. Considering different GHSV conditions and maintaining a constant gas flow, the best performance of ZnO sorbents was achieved at 550–600 °C and 25,000 $h^{-1,}$ reaching an $SC_b$ of around 5.1 g sulphur per 100 g of sorbent after 4.2 h, confirming our previous results.

ZnO sorbents in the presence of wet syngas showed an appropriate performance for HGC, but they also promoted a catalytic response facilitating other reactions such as methane reforming and WGS.

The modeling of the breakthrough curves using the deactivation model explained the influence of different operating parameters (temperature, GHSV, and $H_2S$ concentration), indicating that representative parameters P1 and P2 alter the S-shape curves. In particular, variations in temperature directly affected $k_s$*, while $k_d$ had an inverse change. When GHSV varied, it caused a direct and inverse effect on $k_d$ and $k_s$*, respectively. However, concentration changes showed an inverse influence on both constants.

Considering thermodynamic parameters from the adsorption process, by using the Arrhenius and Eyring–Polanyi expressions, $E_a$ was determined to be around 10 kJ $mol^{-1}$. In contrast $\Delta H$* and $\Delta S$* of the transition state were around 3.5 kJ $mol^{-1}$ and $-0.27$ kJ $mol^{-1}$ $K^{-1}$, respectively. A positive $\Delta H$* means that heat is required to pass from reactants to the transition state, while a negative $\Delta S$* indicates that the degree of disorder of the transition state is lower than that reactant. Finally, the diffusion coefficient and $k_0$ values were calculated for each experimental condition using spherical coordinates in order to understand the process in circumstances similar to reality.

**Supplementary Materials:** The following supporting information can be downloaded at: https://www.mdpi.com/article/10.3390/en16020792/s1, Supplementary material S1: Spherical geometry model of rate constant and diffusion coefficient.

**Author Contributions:** Conceptualization, E.B. and A.D.; methodology, E.B., A.D. and L.D.Z.; validation, A.H. and E.C.; formal analysis, A.D. and E.C.; investigation, E.C., A.D. and A.H.; data Curation, E.C. and A.D.; writing—original draft preparation E.C. and A.D.; writing—review and editing, E.C. and A.D.; supervision, E.B. All authors have read and agreed to the published version of the manuscript.

**Funding:** This research has received funding from the European Union's Horizon 2020 research and innovation program under grant agreement No. 815284 BLAZE project.

**Data Availability Statement:** Not applicable.

**Acknowledgments:** The authors thank the partners of the H2020, BLAZE, and GICO projects and in particular Ilaria Mirabelli and Michael Muller for some suggestions.

**Conflicts of Interest:** The authors declare no conflict of interest.

## References

1. Marcantonio, V.; Bocci, E.; Ouweltjes, J.P.; Del Zotto, L.; Monarca, D. Evaluation of sorbents for high temperature removal of tars, hydrogen sulphide, hydrogen chloride and ammonia from biomass-derived syngas by using Aspen Plus. *Int. J. Hydrog. Energy* **2020**, *45*, 6651–6662. [CrossRef]
2. Meng, X.; De Jong, W.; Pal, R.; Verkooijen, A.H.M. In bed and downstream hot gas desulphurization during solid fuel gasification: A review. *Fuel Process. Technol.* **2010**, *91*, 964–981. [CrossRef]
3. Marcantonio, V.; Del, L.; Pieter, J.; Bocci, E. Main issues of the impact of tar, $H_2S$, HCl and alkali metal from biomass-gasification derived syngas on the SOFC anode and the related gas cleaning technologies for feeding a SOFC system: A review. *Int. J. Hydrog. Energy* **2021**, *47*, 517–539. [CrossRef]
4. Woolcock, P.J.; Brown, R.C. A review of cleaning technologies for biomass-derived syngas. *Biomass Bioenergy* **2013**, *52*, 54–84. [CrossRef]
5. Ud Din, Z.; Zainal, Z.A. Biomass integrated gasification-SOFC systems: Technology overview. *Renew. Sustain. Energy Rev.* **2016**, *53*, 1356–1376. [CrossRef]
6. Cui, C.; Ma, J.; Wang, Z.; Liu, W.; Liu, W.; Wang, L. High performance of mn-doped mg alox mixed oxides for low temperature nox storage and release. *Catalysts* **2019**, *9*, 677. [CrossRef]
7. Górecka, S.; Pacultová, K.; Górecki, K.; Smýkalová, A.; Pamin, K.; Obalová, L. Cu-mg-fe-o-(Ce) complex oxides as catalysts of selective catalytic oxidation of ammonia to dinitrogen (nh3-sco). *Catalysts* **2020**, *10*, 153. [CrossRef]
8. Song, S.; Zhang, S.; Zhang, X.; Verma, P.; Wen, M. Advances in Catalytic Oxidation of Volatile Organic Compounds over Pd-Supported Catalysts: Recent Trends and Challenges. *Front. Mater.* **2020**, *7*, 595667. [CrossRef]
9. Liu, X.; Zhang, Q.; Ye, G.; Li, J.; Li, P.; Zhou, X.; Keil, F.J. Deactivation and regeneration of Claus catalyst particles unraveled by pore network model. *Chem. Eng. Sci.* **2020**, *211*, 115305. [CrossRef]
10. Shen, F.; Liu, J.; Zhang, Z.; Dong, Y.; Gu, C. Density functional study of hydrogen sulfide adsorption mechanism on activated carbon. *Fuel Process. Technol.* **2018**, *171*, 258–264. [CrossRef]
11. Bakker, W.J.W.; Kapteijn, F.; Moulijn, J.A. A high capacity manganese-based sorbent for regenerative high temperature desulfurization with direct sulfur production Conceptual process application to coal gas cleaning. *Chem. Eng. J.* **2003**, *96*, 223–235. [CrossRef]
12. Cheah, S.; Carpenter, D.L.; Magrini-Bair, K.A. Review of mid- to high-temperature sulfur sorbents for desulfurization of biomass- and coal-derived syngas. *Energy Fuels* **2009**, *23*, 5291–5307. [CrossRef]
13. Aravind, P.V.; De Jong, W. Evaluation of high temperature gas cleaning options for biomass gasification product gas for Solid Oxide Fuel Cells. *Prog. Energy Combust. Sci.* **2012**, *38*, 737–764. [CrossRef]
14. Yasyerli, S.; Dogu, G.; Ar, I.; Dogu, T. Activities of copper oxide and Cu-V and Cu-Mo mixed oxides for $H_2S$ removal in the presence and absence of hydrogen and predictions of a deactivation model. *Ind. Eng. Chem. Res.* **2001**, *40*, 5206–5214. [CrossRef]
15. Garces, H.F.; Galindo, H.M.; Garces, L.J.; Hunt, J.; Morey, A.; Suib, S.L. Low temperature $H_2S$ dry-desulfurization with zinc oxide. *Microporous Mesoporous Mater.* **2010**, *127*, 190–197. [CrossRef]
16. Novochinskii, I.I.; Song, C.; Ma, X.; Liu, X.; Shore, L.; Lampert, J.; Farrauto, R.J. Low-temperature $H_2S$ removal from steam-containing gas mixtures with ZnO for fuel cell application. 1. ZnO particles and extrudates. *Energy Fuels* **2004**, *18*, 576–583. [CrossRef]
17. Gupta, R.P.; O'Brien, W.S. Desulfurization of hot syngas containing hydrogen chloride vapors using zinc titanate sorbents. *Ind. Eng. Chem. Res.* **2000**, *39*, 610–619. [CrossRef]
18. Ko, T.; Chu, H.; Liou, Y. A study of Zn–Mn based sorbent for the high-temperature removal of $H_2S$ from coal-derived gas. *J. Hazard. Mater.* **2007**, *147*, 334–341. [CrossRef] [PubMed]
19. Li, L.; Sun, T.H.; Shu, C.H.; Zhang, H.B. Low temperature $H_2S$ removal with 3-D structural mesoporous molecular sieves supported ZnO from gas stream. *J. Hazard. Mater.* **2016**, *311*, 142–150. [CrossRef]
20. Chomiak, M.; Trawczyński, J.; Blok, Z.; Babiński, P. Monolithic Zn-Co-Ti based sorbents for hot syngas desulfurization. *Fuel Process. Technol.* **2016**, *144*, 64–70. [CrossRef]

21. Hatunoglu, A.; Dell'era, A.; Del Zotto, L.; Di Carlo, A.; Ciro, E.; Bocci, E. Deactivation model study of high temperature $H_2S$ wet-desulfurization by using ZnO. *Energies* **2021**, *14*, 8019. [CrossRef]
22. Frilund, C.; Simell, P.; Kaisalo, N.; Kurkela, E.; Koskinen-Soivi, M.L. Desulfurization of Biomass Syngas Using ZnO-Based Adsorbents: Long-Term Hydrogen Sulfide Breakthrough Experiments. *Energy Fuels* **2020**, *34*, 3316–3325. [CrossRef] [PubMed]
23. Zuber, C.; Husmann, M.; Schroettner, H.; Hochenauer, C.; Kienberger, T. Investigation of sulfidation and regeneration of a ZnO-adsorbent used in a biomass tar removal process based on catalytic steam reforming. *Fuel* **2015**, *153*, 143–153. [CrossRef]
24. Kim, K.; Jeon, S.K.; Vo, C.; Park, C.S.; Norbeck, J.M. Removal of Hydrogen Sulfide from a Steam-Hydrogasifier Product Gas by Zinc Oxide Sorbent. *Ind. Eng. Chem. Res.* **2007**, *46*, 5848–5854. [CrossRef]
25. Abdullah, A.H.; Mat, R.; Somderam, S.; Abd Aziz, A.S.; Mohamed, A. Hydrogen sulfide adsorption by zinc oxide-impregnated zeolite (synthesized from Malaysian kaolin) for biogas desulfurization. *J. Ind. Eng. Chem.* **2018**, *65*, 334–342. [CrossRef]
26. Suyadal, Y.; Erol, M.; Oğuz, H. Deactivation model for the adsorption of trichloroethylene vapor on an activated carbon bed. *Ind. Eng. Chem. Res.* **2000**, *39*, 724–730. [CrossRef]
27. Ngoc Lan Thao, N.T.; Chiang, K.Y.; Wan, H.P.; Hung, W.C.; Liu, C.F. Enhanced trace pollutants removal efficiency and hydrogen production in rice straw gasification using hot gas cleaning system. *Int. J. Hydrogen Energy* **2019**, *44*, 3363–3372. [CrossRef]
28. Lancaster, D.K.; Sun, H.; George, S.M. Atomic Layer Deposition of Zn(O,S) Alloys Using Diethylzinc with $H_2O$ and $H_2S$: Effect of Exchange Reactions. *J. Phys. Chem. C* **2017**, *121*, 18643–18652. [CrossRef]
29. Tamhankar, S.S.; Bagajewlcz, M.; Gavalas, G.R.; Sharma, P.K.; Flytzanl-Stephanopoulos, M. Mixed-Oxide Sorbents for High-Temperature Removal of Hydrogen Sulfide. *Ind. Eng. Chem. Process Des. Dev.* **1986**, *25*, 429–437. [CrossRef]
30. Joshi, S.Y.; Ren, Y.; Harold, M.P.; Balakotaiah, V. Determination of kinetics and controlling regimes for $H_2$ oxidation on $Pt/Al_2O_3$ monolithic catalyst using high space velocity experiments. *Appl. Catal. B Environ.* **2011**, *102*, 484–495. [CrossRef]
31. Ko, T. Fitting of breakthrough curve by deactivation kinetic model for adsorption of $H_2S$ from syngas with Zn-contaminated soil. *Asian J. Chem.* **2015**, *27*, 865–869. [CrossRef]
32. Ahmad Farid, M.A.; Hassan, M.A.; Taufiq-Yap, Y.H.; Ibrahim, M.L.; Hasan, M.Y.; Ali, A.A.M.; Othman, M.R.; Shirai, Y. Kinetic and thermodynamic of heterogeneously $K_3PO_4$/AC-catalysed transesterification via pseudo-first order mechanism and Eyring-Polanyi equation. *Fuel* **2018**, *232*, 653–658. [CrossRef]
33. Duan, Y.; Dubouis, N.; Huang, J.; Dalla Corte, D.A.; Pimenta, V.; Xu, Z.J.; Grimaud, A. Revealing the Impact of Electrolyte Composition for Co-Based Water Oxidation Catalysts by the Study of Reaction Kinetics Parameters. *ACS Catal.* **2020**, *10*, 4160–4170. [CrossRef]
34. Nautiyal, P.; Subramanian, K.A.; Dastidar, M.G. Kinetic and thermodynamic studies on biodiesel production from Spirulina platensis algae biomass using single stage extraction-transesterification process. *Fuel* **2014**, *135*, 228–234. [CrossRef]